# Understanding tungsten erosion during inter/intra-ELM periods in He-dominated JET-ILW plasmas

A. Huber[1], S. Brezinsek[1], V. Huber[2], E. Solano[3], G. Sergienko[1], I. Borodkina[4], S. Aleiferis[5], A. Meigs[6], D. Tskhakaya[4], M. Sertoli[6], M. Baruzzo[7], D. Borodin[1], P. Carvalho[8], E. Delabie[9], D. Douai[10], A. Kirschner[1], K. Lawson[6], Ch. Linsmeier[1], J. Mailloux[6], S. Menmuir[6], Ph. Mertens[1], E. Pawelec[11], J. Romazanov[1], A. Shaw[6] and JET contributors*

[1]*Forschungszentrum Jülich GmbH, Institut für Energie- und Klimaforschung - Plasmaphysik, 52425 Jülich, Germany*
[2]*Forschungszentrum Jülich GmbH, Supercomputing Centre, 52425 Jülich, Germany*
[3]*Laboratorio Nacional de Fusión, CIEMAT, Madrid, Spain*
[4]*Institute of Plasma Physics of the CAS, Prague, Czech Republic*
[5]*NCSR 'Demokritos' 153 10, Agia Paraskevi Attikis, Greece*
[6]*CCFE, Culham Science Centre, Abingdon, OX14 3DB, UK*
[7]*ENEA for EUROfusion, via E. Fermi 45, 00044 Frascati (Roma), Italy*
[8]*Instituto de Plasmas e Fusão Nuclear, Instituto Superior Técnico, Universidade de Lisboa, Portugal*
[9]*Oak Ridge National Laboratory, Oak Ridge, TN 37831-6169, USA*
[10]*CEA, IRFM, F-13108, Saint-Paul-Lez-Durance, France*
[11]*Institute of Physics, University of Opole, Opole, Poland*

E-mail: A.Huber@fz-juelich.de

Keywords: helium plasma, tungsten erosion, tungsten divertor, optical emission spectroscopy, plasma-material interactions, JET-ILW

PACS: 52.70.Kz, 52.25.Vy, 52.40.Hf, 52.55.Fa, 52.25.Fi

## Abstract

Tungsten erosion was quantified during inter/intra-ELM periods in He-dominated JET-ILW plasmas by optical emission spectroscopy. The intra-ELM tungsten sputtering in helium plasmas, which dominates the total W source, prevails by a factor of about 4 over inter-ELM sputtering in the investigated ELM frequency range from 90 Hz-120 Hz. He ions are mainly responsible for the W erosion during the ELMs in He plasmas. The strong in/out asymmetry of the ELM-induced W erosion is observed in He plasmas even at high ELM frequencies beyond 100 Hz. In Ohmic/L-mode plasmas and during the H-mode inter-ELM plasma phases both $He^{2+}$ and $Be^{2+}$ ionic species are major contributors to the W erosion. Their contribution depends on the electron temperature in the divertor: for $T_e > 15$ eV both species cause significant W sputtering, for $T_e < 15$ eV, $Be^{2+}$ ions are solely responsible for the W erosion. Tungsten erosion during in both inter and intra-ELM periods in He-dominated plasmas are significantly larger than in deuterium plasmas. It is 15-25 times larger during the inter-ELM phase and in L-mode discharges at $T_e$= 25-30 eV. On the other hand, the ELM-induced W source is by a factor of 3 larger than in D plasmas.

*See the author list in: J. Mailloux et al., 28th IAEA FusiEnergyConference2020 (May 2021)

## 1. Introduction

Tungsten (W) is foreseen as plasma-facing material (PFM) for the divertor in the next step fusion plasma device, ITER [1]. W is selected because of its high threshold energy for physical sputtering [2], good power-handling capabilities with high melting point [3] and low retention of radioactive tritium (T) in the plasma-facing components (PFCs) [4,5]. The erosion of tungsten can seriously limit the lifespan of the respective components of the first wall [6]. On the other hand, the tungsten influx into the confined region can lead to a dilution of the core fusion plasma and increased energy losses through radiation, which in turn could have a decisive impact on the plasma performance [7,8]. The mechanism of tungsten erosion is mainly determined by the material of the surfaces of the first wall, which is the source of the main impurities in the plasma, and by the choice of the fuelling gas. By exchanging deuterium (D) for helium (He) in a machine with ITER-like wall which contains Be and W materials, the effect of the fuel gasses on the character of edge and divertor physics such as the W erosion and nature of the Be impurity source can be studied.

Operation of H-modes in helium-4 plasmas (He plasmas) is intended as one option for the low activation phase of ITER in order to develop plasma scenarios for the future deuterium-tritium (DT) operation as well as to commission the operationally relevant ITER systems and the plasma diagnostics in a friendly non-nuclear environment [9]. In addition, the alpha particles generated in DT fusion reactions in the active phase of ITER reinforce the demand for a detailed understanding of the interaction processes between He and W. To date, however, most of the plasma-wall interaction studies in tokamaks with a completely metallic wall, such as JET [10] and ASDEX Upgrade (AUG) [11], have been executed in deuterium (D) or protium (H) plasmas. Pure He plasmas make up a negligible portion of the discharges carried out in these tokamaks [12].

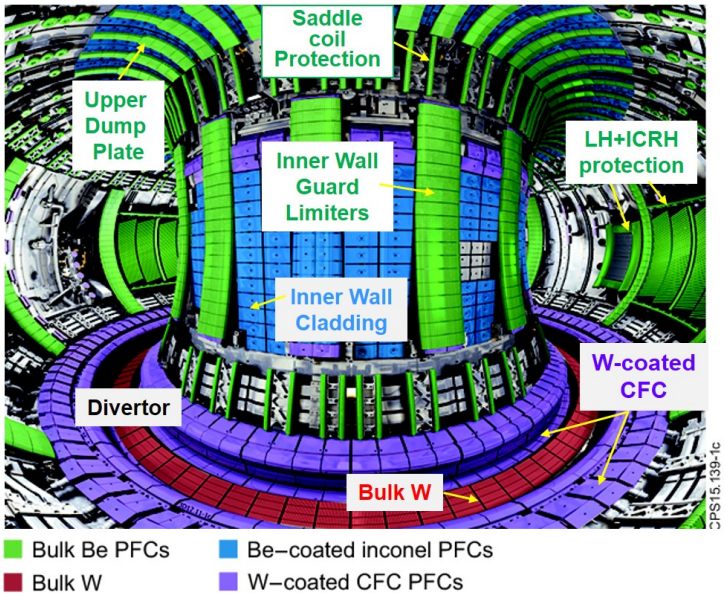


Fig 1 Annotated photo of the ITER-like wall with the material configuration.

An intensive He campaign at JET-ILW is planned for 2021 after the DTE2 campaign. To get the urgently needed information

about the He plasmas, such as the L-H transition threshold or some aspects of PWI physics, a short campaign with He plasma discharges and D-neutral beam injection (D-NBI) was carried out during the recent JET campaign [13].

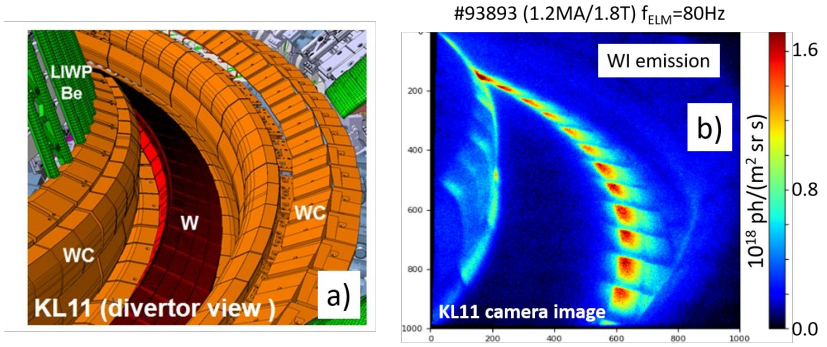


Fig.2 a) Field of View (FoV) of the divertor spectroscopy camera, b) single frame of the intensified camera system dominated by the intra-ELM tungsten sputtering.

This paper focuses on the analysis of the gross erosion of tungsten during inter/intra-ELM periods in the inner and outer legs of the JET-ILW divertor in the He-dominated H-mode as well as L-mode plasmas.

## 2. Methods for W erosion evaluation in the JET-ILW divertor

The identification of the W atomic sources was performed at the JET tokamak with the ITER-like wall (JET-ILW) by means of optical emission spectroscopy (OES). This is mainly based on the observation of the most prominent WI transition ($5d^5(^6S)6s\ ^7S_3 \rightarrow 5d^5(^6S)6p\ ^7P_4^o$) at $\lambda$ = 400.9 *nm* of the sputtered W atoms with the aim of determining gross erosion. Fig. 1 shows the material configuration of the JET-ILW tokamak first wall. Bulk tungsten and tungsten coatings on carbon fibre reinforced carbon (CFC) substrates are used in the area of the divertor (see also Fig.2a), which is subject to high heat loads. The main chamber consists of beryllium coatings on Inconel alloy 625 and bulk beryllium limiter tiles.

Particle fluxes of sputtered W atoms, $\Gamma_W$, are gained from line-of-sight integrated photon fluxes, $I_{WI}$, by applying inverse photon efficiencies, *S/XB,* which are determined by the multi-machine scaling law [14,15,16]:

$$\Gamma_W = 4\pi \frac{S}{XB}(T_e) \cdot I_{WI}\,, \tag{1}$$

$$S/XB\,(T_e) = 53.63 - 56.07 \times e^{(-0.045 \times T_e[eV])} \tag{2}$$

The S/XB values during the inter-ELM periods as well as in L-mode plasmas result from an electron temperature, $T_e$, which is determined by an array of divertor Langmuir probes (LP). In the intra-ELM phase, electron temperatures of $T_e$ = 70-100 eV are assumed at the strike points (SPs) , which provide S/*XB* values of ≈50 according to equation 2. Note that the inverse photon efficiencies, S/*XB,* in the $T_e$-range between $T_e$=50 eV and $T_e$=200 eV are only weakly

dependent on the electron temperature $T_e$: they increase slightly from the value of 48 to 53.6. Hence, the evaluation of the particle fluxes of sputtered W atoms is insensitive to our assumption of fixed value of *S/XB* = 50. Similar values for S /XB (=50) for the intra-ELM periods were used in [6,17,18].

Three approaches with a new algorithm for subtracting the continuum plasma radiation were applied in this study to achieve a quantitative measure of W erosion in both the outer and inner divertor area:

1) the combination of two spectroscopic systems, the divertor spectroscopy system (KT3) and the W photomultiplier filterscope diagnostics (PMT), with good spectral and temporal resolution. Fig.3 shows the poloidal cross section of the JET-ILW divertor with the lines of sight (LOS) of the KT3 divertor spectroscopy system (Fig.3a) and of the PMT filterscope diagnostic (Fig.3b). The PMT filterscope has circular lines of sight with a diameter of 380 mm each, covering the entire inner and outer divertor. The KT3 system consists of 22 lines-of-sight (LOS) covering about 320 mm of the outer divertor. Each LOS has a toroidal extension of 2 mm and a poloidal dimension of 14.5 mm at the divertor targets. The system has a time resolution of 40 ms and covers with three Czerny-Turner spectrometers the spectral range of 200-1100 nm ;

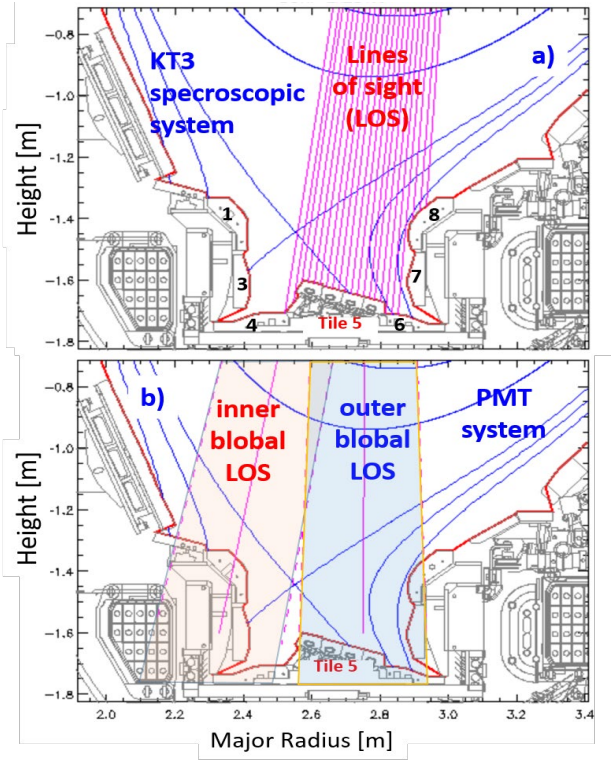


Fig.3 Poloidal cross-sections of the JET-ILW divertor with lines of sight (LOS) of the KT3 divertor spectroscopy system (a) and of the PMT filterscope diagnostic (b)

2) the second approach is based on the calculation of the accumulated photon flux, $\int I_W dt$;

3) an approach based on spectroscopic imaging using two digital cameras with an identical field of Fiew (FoV) (shown in Fig.2a), equipped with interference filters (IFs) of different bandwidths (FWHM) centred on the neutral tungsten emission line W I (400.9 nm).

These methods allow distinguishing the erosion sources of W in the intra-ELM period from that in the inter-ELM period. The detailed description of these three approaches are given in the [19] paper.

## 3 Experimental Results

### *3.1 Experiment in He plasmas*

Identification of erosion sources in He plasmas is one of the important research topics of the plasma-wall interaction. This study was recently carried out on $^4$He plasmas in the JET-ILW with $B_t$=1.8 T, Ip=1.2-1.7 MA and was compared with D plasmas. The additional input power is introduced in the He plasmas by the Deuterium Neutral Beam Injection ( D-NBI). In order to ensure minimal contamination of the He plasmas in this study, the examined pulses were only carried out with He gas injection (no injection of hydrogenic species). Fig.4 shows the time traces of an H-mode He discharge in JET-ILW with $B_t/I_p$=1.8 T/1.2 MA in low-triangularity magnetic equilibria (average triangularity of δ=0.22) with the outer strike point located on the horizontal divertor plate (the so-called tile 5). During the He pulses, the divertor cryopump operated as usual, removing hydrogenic species. Argon frosting was not used to pump the helium gas. With sufficient NBI heating power, the coherent M mode is observed at the L-H transition. A similar finding was made earlier in the hydrogen and D plasmas [20]. As the input power increases, small ELMs appear, an effect which is mixed with the M-mode followed by isolated large ELMs, described here as Type I ELMs [13]. Fig.2b shows the single frame of the intensified camera system dominated by the intra-ELM tungsten sputtering measured during the Type I ELMs phase.

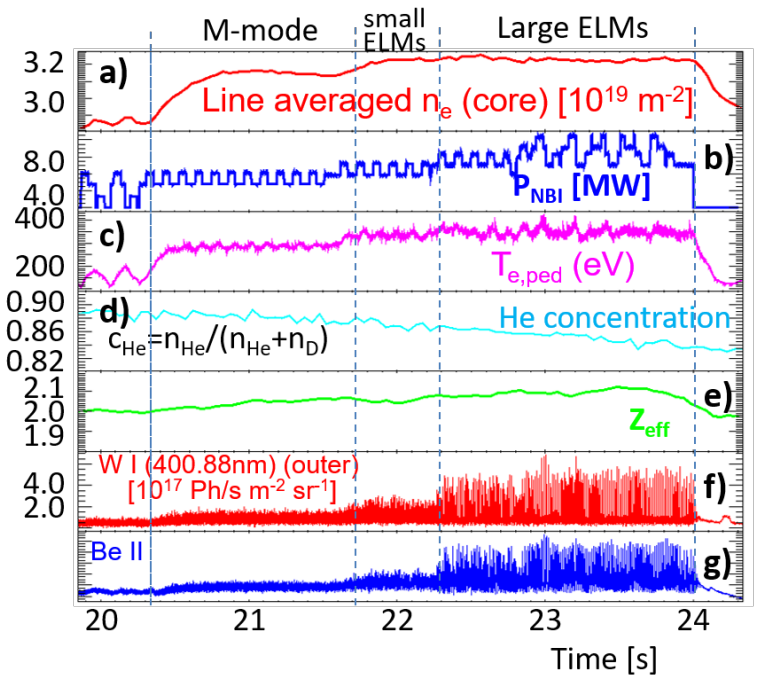


Fig.4 Time traces of a) central line averaged $n_e$, b) D-NBI heating power, c) electron temperature at the pedestal $T_{e,ped}$, d) Helium concentration, e) the effective ion charge $Z_{eff}$, f) *WI*- and g) *BeII* fast emission signal in the outer divertor.

Based on Langmuir probe (LP) measurements at the outer strike point during the inter-ELM periods, the electron temperature was in the range of $T_e$ = 24–28 eV. The examined He plasmas are characterized by a high ELM frequencies (90-130 Hz) and low pedestal electron temperatures of $T_{e,ped}$ < 400 eV and $Z_{eff}$ is kept in the range of 2.05-2.1. It demonstrates a plasma stored energy ($W_{dia}$) of ≈1.1 MJ with an ELM energy loss of $\Delta W_{ELM}$≈ 0.12 MJ (the loss of

stored plasma energy during the ELM). The $P_{sep}$ ( $P_{sep} = P_{\Omega} + P_{NBI} - \frac{dW_{dia}}{dt} - P_{rad}^{bulk} = P_{loss} - P_{rad}^{bulk}$ ) required to reach the type I ELMs in He is of the order of 4-5.5 MW, which is 2-2.5times the L-H transition threshold value of 2.2 MW. Measurements of He, D, and H concentrations in the JET sub-divertor region are carried out with Optical Penning Gauge Spectroscopy [21,22]. During the D-NBI injection, the concentration of He, $c_{He}=n_{He}/(n_{He}+n_D+n_H)$ decreases slightly with the pulse evolution and the mean value of $c_{He}$ over the Type I ELM phase type was about 0.85. The measurements confirm the presence of mixed He-dominated plasmas.

*3.2 Intrinsic impurities in He plasmas*

Similar to the D plasmas, the dominant intrinsic impurity in JET-ILW-He plasmas is Be. Be is produced by the erosion of the first wall made of beryllium by fuel ions and charge exchange neutrals [10]. The remaining C concentration in these plasmas was about $c_C \approx 0.07\%$, which is at least one order of magnitude lower than Be concentration. These mixed helium/deuterium (85%/15%) plasmas demonstrated an effective ion charge of $Z_{eff} = 2.07 \pm 0.03$, mainly determined by Be impurity. The pure mixed (He / D) plasmas without impurities should have $Z_{eff} = 1.92$. Therefore, the $\Delta Z_{eff}$ observed in our experiments is 0.12-0.18, which corresponds to a Be concentration of 3% to 4.0%. The impurity flux towards the W divertor is determined by optical emission spectroscopy. For the calculation of the Be concentrations, the Be II (527 nm) spectral line is used. The measurements result in values between 3.2% and 3.8% related to the ion saturation flux: $\frac{\Gamma_{Be}}{\Gamma_{ion}} = \frac{\Gamma_{Be}}{J_{sat}^{ion}/\bar{Z}e} = \frac{4\pi I_{Be}\,(527\text{ nm})S/XB}{J_{sat}^{ion}/\bar{Z}e}$, where $\bar{Z}$ is the averaged charge of this mixed He/D plasmas and the S/XB factor for the Be II (527 nm) emission line is about 65 in the $T_e$ range 25-30 eV and $n_e=5\times 10^{19}$ m$^{-3}$. Similar results are achieved $\frac{\Gamma_{Be}}{\Gamma_D} = \frac{I_{Be}\,(527\,nm)S/XB}{I_{D\alpha}\,S/XB}\,c_D \approx 0.032 \div 0.036$ and $\frac{\Gamma_{Be}}{\Gamma_{He}} = \frac{I_{Be}\,(527\,nm)S/XB}{I_{He}(668\,nm)\,S/XB}\,c_{He} \approx 0.035 \div 0.037$ taking into the account the concentrations of $c_D=15\%$ and $c_{He}=85\%$ and using the following S/XB values: 15 and 120 for the emission lines $D_\alpha$ and He I (668 nm), respectively. The S/XB values used here were taken from the ADAS database [23]. In the following analysis, we will use the $c_{Be}$ values of 3.5%.

*3.3 Charge state distribution of impurities and helium*

The sputtering process depends strongly on the charge state of the impinging ions. It is therefore important to know the charge state distribution of impurities and He ions, which is defined by the ionization, recombination and transport processes of impurities and He ions in plasmas [24]. In the coronal equilibrium the distribution of the impurity particles amongst the different charge states is purely a function of $T_e$, with no dependence on $n_e$. At the plasma edge, however, the local coronal equilibrium cannot be supposed for the calculation of the charge state distribution. Typically, the plasma in a non-coronal equilibrium can be well described by the product of two plasma parameters, the electron density and the residence time, $n_e \times \tau$ [25,26].

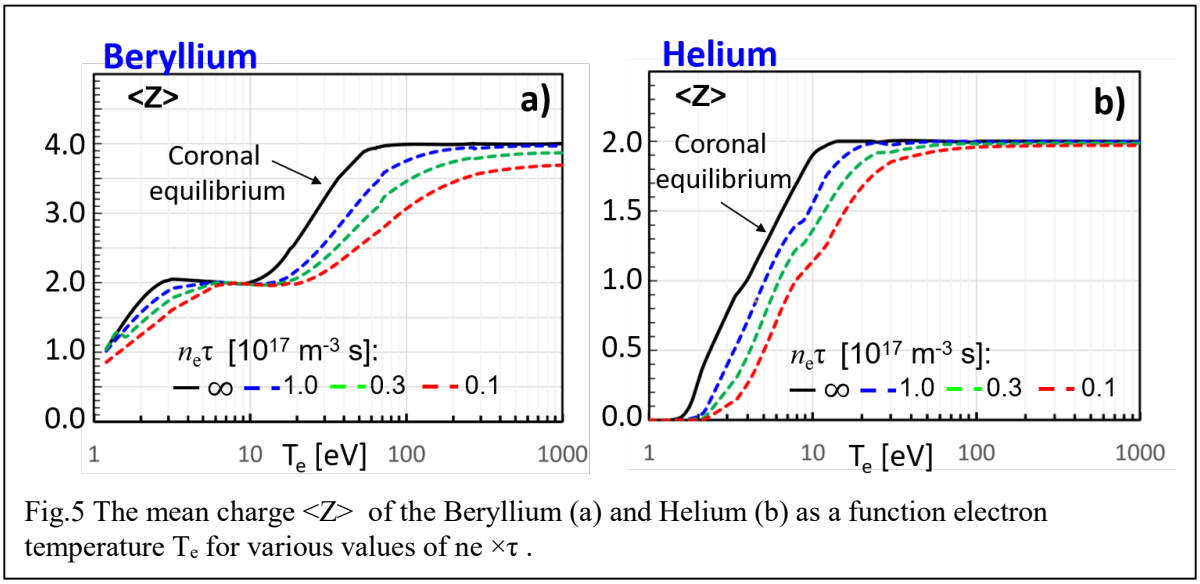


Fig.5 The mean charge <Z> of the Beryllium (a) and Helium (b) as a function electron temperature $T_e$ for various values of ne $\times\tau$ .

Fig. 5 shows the mean charge <Z> of beryllium and He as a function electron temperature $T_e$ for various values of $n_e \times \tau$ . In this contribution we use polynomial fits applied in [27] which were evaluated with help of ADAS for $n_e = 10^{20}$ $m^{-3}$, which is a typical value for the scrape-off layer (SOL) in the divertor region. One can see from the Fig. 5 that the mean charges of Be and He are $\langle Z \rangle^{Be}$ = 2.0-2.2 and $\langle Z \rangle^{He}$ = 1.85 for typical values of the non-coronal parameter of $n_e \times \tau = 0.3 \times 10^{17}$ $m^{-3}$ s and for the $T_e$=24-28 eV measured by the LPs during the inter-ELM phase,. During the ohmic phase at the $T_e$ =10 eV the mean charges are: $\langle Z \rangle^{Be}$ = 2.0 and $\langle Z \rangle^{He}$ = 1.2 for Be and He respectively..

*3.4 Physical sputtering of W: role of impurities and fuel species*

The major erosion mechanism of tungsten in tokamaks is physical sputtering, which can be calculated with the static-dynamic TrimSP package (Monte-Carlo code SDTrimSP [28] using

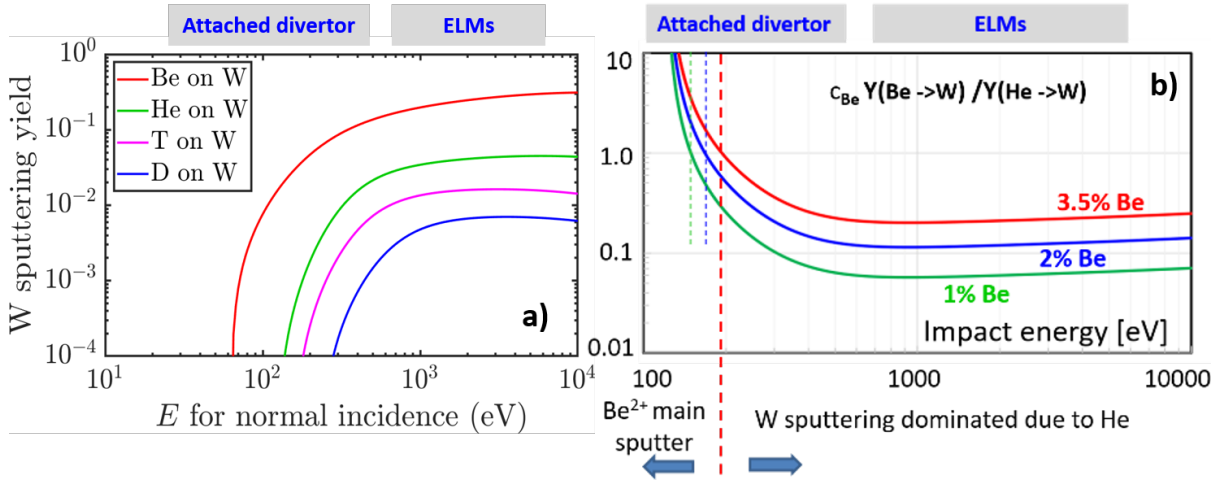


Fig.6 a) the calculated sputtering yields as function of the impact energy at normal incidence b) ratio of the sputtered W atoms by Be and He at different Be concentrations: $c_{Be}$=1%, 2% and 3.5%.

the Eckstein fitting formula, [29].) under assumption of a smooth target surface. Fig.6a shows the calculated physical sputtering yields of tungsten atoms by impinging hydrogenic (D and T), He and Be particles at normal incidence as function of the mono-energetic impact energy, $E_{in}$, of the projectiles. One can see that the sputtering yield by He is more than an order of magnitude greater than by D at the relevant divertor temperatures under the attached conditions. Fig.6b shows the ratio of the sputtered W atoms by Be and He at different Be concentrations: $c_{Be}$ = 1%, 2% and 3.5%. At the impact energy of 1 keV, which is the typical energy of the impinging ions during ELMs, the ratio is about 0.2. This value shows that the main intra-ELM sputter is He, not Be. In contrast to the intra-ELM phase, during the inter-ELM phase and L-mode the contributions of both species, Be as well as He, are significant depending on the divertor $T_e$: for the $E_{in}$ > 180 eV, main channel of sputtering is due to sputtering by He and for the $E_{in}$ < 180 eV, is due to Be. For twice ionised Be and He the $E_{in}$ = 180 eV corresponds to the $T_e$ of ≈ 22.5 eV.

*3.5 Tungsten Erosion during the inter-ELM phases*

The W photomultiplier filterscope diagnostics (PMT) on JET [30] collects W I (400.9 nm) emission light conducted to Photo Multiplier Tubes (PMTs) via optical fibres with a time response of 10 kHz. It is able to resolve the high ELM frequency, of order of 100 Hz, observed in He plasmas. The disadvantage of this diagnostics is the collection of the W line emission along with the plasma continuum during the detection. The contribution of the latter is of the same order as or even larger than the W I line emission.

The combined detection of the W I emission with spectroscopic systems, PMT[30] and KT3[31] with good temporal and spectral resolution, respectively, enables both contributions to be separated [19]. In order to evaluate the intensity of the plasma background continuum, the photon fluxes of these two measurements are compared during the flat-top phases of the analyzed discharge, as shown in Fig. 7. To compare these two measurements, the filterscope diagnostic signal (PMT) is integrated over a time window of 40 ms, which is similar to the time exposure of KT3 spectroscopy, and corrected by taking into account the geometry of the KT3 lines of sight. Fig. 7 demonstrates the linear correlation between two signals, PMT and KT3, with a clear offset, $I_{offset}$ = 4.82×10$^{16}$ ph/(s m$^2$ sr), in the W filterscope (PMT) measurements which is due to the plasma continuum. Bremsstrahlung (free-free transition) mainly contributes to the measured plasma continuum. The subtraction of the offset results in $I_{WI}$ ≈ 2.5×10$^{16}$ ph/(s m$^2$ sr), which corresponds to the inter-ELM-induced W sputtering of 6.7×10$^{19}$ atoms/s integrated over the entire area of the outer strike point. Here an S/XB ratio of 37 is taken into the account (for $T_e$=30 eV).

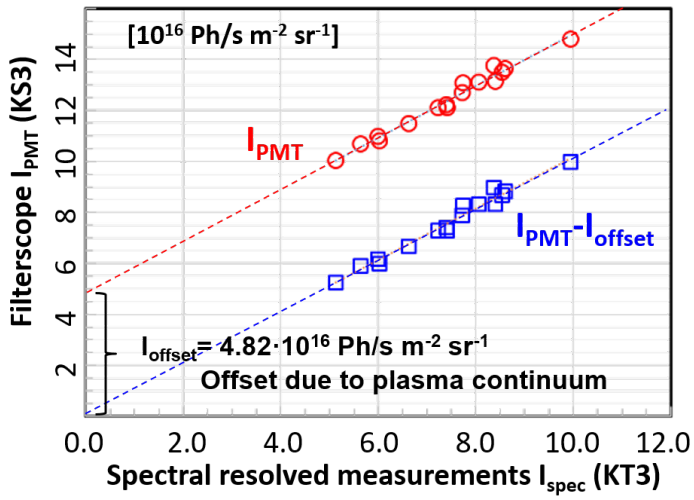


Fig.7 Linear relation between filterscope (PMT) and spectroscopy (KT3) signals. The offset in the PMT measurements is ascribed to the plasma continuum radiation.

*3.6 W Erosion during the intra-ELM phases*

The accumulated photon flux $\int I_W dt$ is used to assess the erosion fluxes of W during the intra-ELM phases. This method could provide the clear separation of the ELM induced W sputtering fluxes from the inter-ELM-phase [19]. Fig.8 shows time traces of the accumulated photon fluxes $\int I_W dt$ collected from the outer and inner divertor legs. The time evolution of the photon fluxes $I_W$ are also shown. The $\int I_W dt$ signal shows the slope between the ELMs, which is determined by the photon fluxes from the W-sputtered atoms as well as by the plasma continuum.

The accumulated photon flux demonstrates a jump in the signal during an ELM event. The height of this jump defines the number of emitted WI photons during the single ELM. For the

ELM event shown in Fig.8, approximately $1.3\times10^{18}$ atoms per ELM and $2.53\times10^{18}$ atoms per ELM are eroded in the inner and outer divertor legs, respectively. These values correspond to the W sources of $1.3\times10^{20}$ atoms/s and $2.53\times10^{20}$ atoms/s for ELM frequency of $f_{ELM}$ = 100 Hz. Thus, the intra –ELM W source is in the outer divertor is larger than the source during the inter-ELM phase, of $6.7\times10^{19}$ atoms/s, evaluated in the section 3.5. We can conclude that the intra-ELM tungsten sources in He plasmas, analogously to the D plasmas, dominate the total W source. In the examined ELM frequency range of 90 Hz-120 Hz, the intra-ELM sputtering outweighs inter-ELM sputtering by a factor of about 4. Figures 9a and 9b

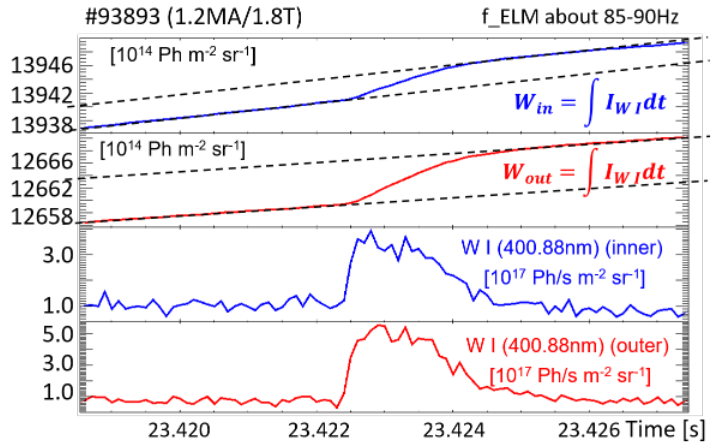


Fig.8 Time traces of the accumulated photon flux, $\int I_W dt$, as well as the WI photon flux density in the inner and outer divertor.

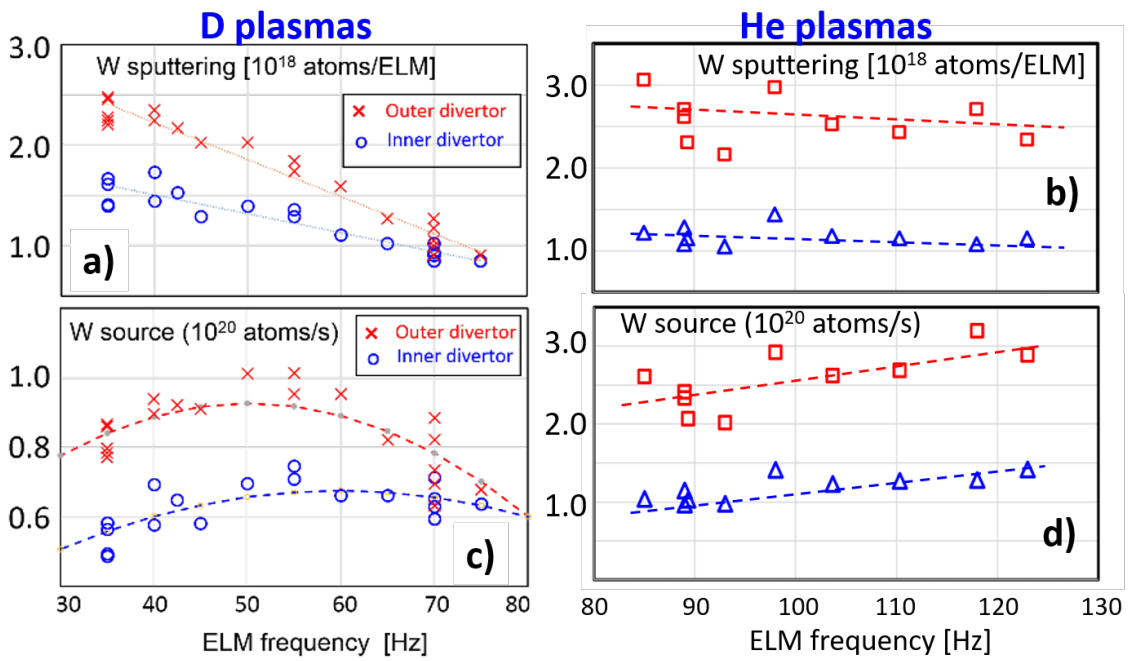


Fig.9 The quantity of the sputtered W atoms per single ELM event in the inner and outer divertor regions in D (a) and He (b) plasmas. The outer (red symbols) and inner (blue symbols) divertor tungsten sources as function of the $f_{ELM}$ in D (c) and He ( d) plasmas.

show the number of eroded tungsten atoms as function of the frequency $f_{ELM}$ in D and He plasmas. Here the total amount of eroded W atoms in the outer (inner) divertor region is calculated by integration over the entire area of the outer (inner) strike point. It should be noted that in the small number of the examined He plasmas the H-mode plasmas show relatively high

ELM frequencies and we do not have information about the W sputtering for $f_{ELM}$ below 80 Hz. One sees that the W sputtering and sources in the He plasmas are significantly larger than in D plasmas. The outer divertor W source is higher by more than a factor of 3 in the He plasmas than in D. In D plasmas, the inner/outer asymmetry of the tungsten erosion decreases sharply with the ELM frequency, showing an almost symmetrical W erosion source in both divertor regions at frequencies beyond 70 Hz. In contrary to the D plasmas, the He plasmas show strong in/out asymmetry in the W sputtering as well as in W source even at high ELM frequencies beyond 100 Hz. At $f_{ELM} \approx 100$ Hz the outer divertor cross W source is larger by a factor of about 2.

*3.7 Tungsten sputtering yields in Ohmic/ L-mode plasmas and in H-mode inter- ELM plasma phases*

Figure 10 shows the evaluated tungsten gross erosion yields in JET-ILW He plasmas. We should mention from the beginning that the contribution of the $He^+$ to W sputtering is negligible. A significant fraction of the $He^+$ in He plasma is expected for the $T_e$ below 10 eV. But as mentioned in section 3.4 the dominant sputtering of W for $E_{in}$ < 180 eV (below the $T_e$=22.5 eV if we consider the twice ionised ions,) is due to Be. For the calculation of the W sputtering yields in the $T_e$ range beyond 20 eV, where the $He^{2+}$ is the major W sputterer, the tungsten particle flux is normalized to the total $He^{2+}$ ion flux measured by Langmuir probes in the corresponding divertor legs. The saturation ion current collected by LP can be written as

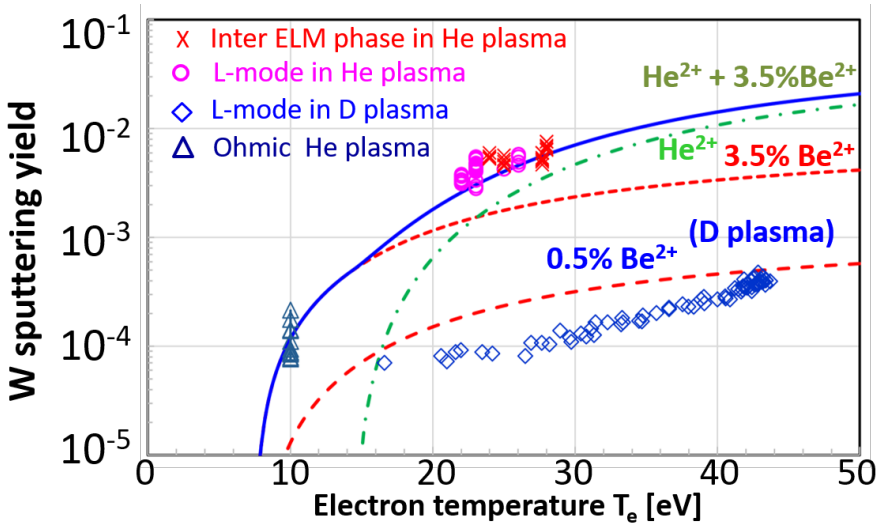


Fig.10 Tungsten sputtering yields measured in the outer divertor in ohmic and L-mode He plasmas as well as during the H-mode inter- ELM periods. The experimental yields compared with the calculated SDTrimSP yields.

$$J_{sat}^{ion} = A \sum_j eZ_j \, n_{js} \, v_{jB} \qquad (2)$$

where A is the area of the probe, $n_{jS}$ is the density of the Zj ion charge at the edge of the sheath and $v_{jB}$ its Bohm-velocity.

Riemann proposed a Generalized Bohm Criterion for a multi-species plasmas [32]. There are two solutions that satisfy the Generalized Bohm Criterion:1) ions reach their individual Bohm velocity at the sheath edge and 2) ions reach the common sound speed, $c_S$. An expression for the common sound speed, $c_S$, for plasmas with multiple ion species was determined by Tokar [33]:

$$c_S = \sqrt{\frac{\sum_{i=0}^{k} \Gamma_i (Z T_e + T_i)}{\sum_{i=0}^{k} \Gamma_i m_i}} \quad (3)$$

where $\Gamma_i$ represents the specific flow of one plasma species out of the κ plasma species. Experiments in two ion species plasmas gave ion speeds that is in agreement with the mentioned second solution [34]. Therefore we are going to use solution two, with common sound speed, here.

Given the $D^+$, $He^+$, and $He^{2+}$ ions collected, this can be expressed by:

$$J_{sat}^{ion} = An_D e c_S + An_{He+} e c_S + n_{He^{2+}} Z(=2) e c_S = Ze\, n_{He^{2+}} c_S \left(1 + \frac{n_D}{Z\, n_{He^{2+}}} + \frac{n_{He^+}}{Z\, n_{He^{2+}}}\right) \quad (4)$$

$$\frac{J_{sat}^{ion}}{Ze} = \Gamma_{He^{2+}} \left[1 + \frac{n_D}{Z\, n_{He^{2+}}} + \frac{n_{He^+}}{Z\, n_{He^{2+}}}\right] = \Gamma_{He^{2+}} [1 + cor_D + cor_{He1+}] \quad (5)$$

where $m_D$ and $m_{He}$ are masses of the D and He ions, $cor_D$ and $cor_{He1+}$ are contribution fractions of the D and $He^{1+}$ ions to the $J_{sat}^{ion}$. They are $cor_D$=0.11÷0.1, $cor_{He^+}$=0.125÷0.06 for the $T_e$ =24-30 eV measured during the inter-ELM phase. From Eq.(4) follows the expression for the $\Gamma_{He^{2+}}$:

$$\Gamma_{He^{2+}} = \frac{J_{sat}^{ion}}{Ze} \frac{1}{(1 + cor_D + cor_{He^+})} \quad (6)$$

The total $He^{2+}$ ion flux collected by LPs in the outer divertor is used for the normalization of the total sputtered W fluxes in the outer divertor to get the W sputtering yield. The results are plotted in Fig. 10 for the inter-ELM phases as well as for the L-mode periods as a function of the divertor $T_e$ measured by the LPs. Also results of the ohmic phase of the He discharges are plotted in this figure (data at $T_e \approx 10$ eV). It should be noted that the measured eroded flux in the ohmic plasma at such a $T_e$ can only be ascribed to $Be^{2+}$ ions and not to He ions. These W fluxes are therefore normalized to the total averaged ion flux, $< \Gamma_{ion} >= \frac{J_{sat}^{ion}}{\overline{Z}e}$, where $\overline{Z}$ is averaged charge of the mixed He/D plasmas ($\overline{Z}$=1.1 for the $T_e$=10 eV). For comparison, the calculated sputter yields are indicated for $He^{2+}$ ions and an admixture of several concentrations of $Be^{2+}$. A good agreement is found between the experimentally obtained yields and the theoretical yield curve (sum of the $He^{2+}$ and 3.5% of $Be^{2+}$). From the shown result we can conclude that sputtering yield curve for W can be described by erosion caused by $He^{2+}$ and $Be^{2+}$ ionic species:

their contribution depends on the divertor $T_e$: for $T_e$=20-28 eV both species significantly contribute for W sputtering, for $T_e$ < 15 eV, $Be^{2+}$ ions are solely responsible for the W erosion. Additionally, Fig.10 shows the result of the W erosion yields achieved in D plasma and published in [14]. The sputtering yield for He plasmas is higher by a factor of 15-18 than in D plasmas. In He plasmas the Be erosion on the first wall is enhanced by the sputtering due to He ions resulting in the larger flux of Be: 3.5% in contrast to the 0.5% in D plasmas. This in turn also leads to an increase in the W erosion through Be ions. Note that some moderate contribution of the $Be^{3+}$ to the W sputtering for $T_e$ beyond 25 eV is expected. However, the modelling shows that the calculated sputtering yield, which takes into account the change in the ionization stage of the impinging Be from $Be^{2+}$ to $Be^{3+}$ at a constant $c_{Be}$ = 3.5% , does not differ significantly from the sputtering yield assessed by 3.5% of $Be^{2+}$ alone: the deviation is below 5% in the W sputtering yield.

The impact energy of the incoming ions are typically expressed in the D plasmas as $E_{in} = 2k_BT_i + 3Z_i k_BT_e$, where $k_B$ is the Boltzmann constant and the $Z_i$ is the charge of the impinging ions. The last term in the $E_{in}$ expression represents the gain energy of the ions through the Debye sheath due to ions acceleration and is defined by the electrical potential drop in the sheath: the electrical potential drop is $V_{sf} \approx 3k_BT_e$ in the D plasmas. This voltage drop depends, however on the mass as well as the Z of the plasma. It could be extracted from the condition of the zero current on the wall (floating conditions when the wall sits at 'floating potential' $V_{sf}$ [35]). Setting $ZeГ^i_{target} = eГ^e_{target}$ gives:

$$\frac{eV_{sf}}{kT_e} = 0.5 \ln\left[\left(\frac{2\pi m_e}{m_i}\right)\left(Z + \frac{T_i}{T_e}\right)\right] \quad (6)$$

where $m_i$ is the ion mass of the fuel species. Thus the voltage drop in the sheath for "$He^+$ dominated plasma" is $3.18k_BT_e$ ($E_{in} = 2k_BT_i + 3.18Z_ik_BT_e$) and about $3k_BT_e$ (corresponding $E_{in} = 2k_BT_i + 3.0Z_i k_BT_e$ ) for the plasma with $He^{2+}$ dominant fraction. It is assumed here that $T_i$=$T_e$.

*3.8 Intra- ELM contributions to the W gross erosion in the divertor*

The free streaming model reveals that ELM-induced tungsten erosion depends almost entirely on the density, $n_{ped}$, and temperature, $T_{ped}$, of the pedestal. In order to maintain the quasi-neutrality, the electrons transfer their parallel energy $E_{e,\parallel}$ to ions during the ELMs on the way to the divertor target [36]. The resulting ions during the ELMs are almost mono-energetic with impact energy, $E_{in}$, up to 4.23 × $T_{e,ped}$. This energy is thus in the keV range, as observed experimentally in [37], and is sufficient to lead to significant sputtering of the W divertor targets. As show in section 3.4, the W sputtering for such energies and correspondingly during the ELMs dominates due to He.

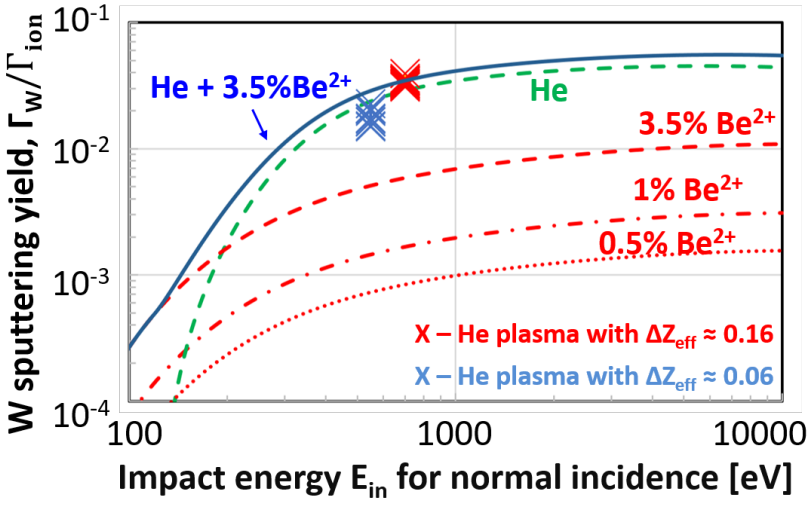


Fig.11 The intra-ELM W sputtered yields measured in helium H-mode plasmas and compared with the calculated yields (solid and dashed lines).

Recently, Borodkina et al. developed an analytical model [38] to evaluate the tungsten-sputtered influx and to interpret the LPs measurements. This analytical model describes well the intra-ELM W-sputtering source as a function of the electron temperature at the pedestal ($T_{e,\,ped}$). According to the analytical model, which takes into the account the evolution of the $T_{e,\,ped}$ drop during the ELM event, the average incident energy of ions, $< \boldsymbol{E_i} >$ is lower than $E_{i,max}=4.23 \times T_{e,ped}$. and is roughly 2×$T_{e,ped}$. The comprehensive modeling of tungsten erosion in the divertor area started recently with the help of the kinetic BIT1 - PIC MC flux tube code. The preliminary result of this modeling also predicts the averaged $< \boldsymbol{E_i} >$ of about 2×$T_{e,ped}$ [39]. The total number of $He^{2+}$ ions per ELM event collected by LPs is used for the normalization of the ELM sputtered W atoms to get the W sputtering yield. The results are plotted in Fig. 11 for the intra-ELM phase. The average incident energy of ions, $<E_i>$ is assumed here to $<E_i>=2\times T_{e,ped}$. As Fig.11 shows, an excellent agreement is found between the experimentally observed results and the theoretical yield curves. W is mainly eroded during the ELMs by energetic He ions with some moderate contribution (about 20%) of the Be ions.

**Conclusion**

In this article we report on recent experiments for the study of the tungsten sources in Ohmic/L-mode as well as in H-mode He-dominated plasmas at JET-ILW, heated with deuterium neutral beam injection (D-NBI). The He and H+D concentrations were measured spectroscopically using the ratio of $^4$He and D lines in an Optical Penning gauge in the subdivertor. In the investigated cases the He concentration was $n_{He}/(n_{He}+n_D+n_H) \approx 85\%$. Three evaluation methods are used to deliver a quantitative evaluation of the W-sputtering in the divertor areas and to distinguish the erosion source in the inter-ELM period from that in the intra-ELM period.

Similar to the D plasma case, the dominant W erosion mechanism in He plasmas is the intra-ELM sputtering induced by ions with impact energies, $E_{in}$, defined by the pre-ELM pedestal temperature. The intra-ELM sputtering in He plasmas prevails by a factor of about 4 over inter-ELM sputtering in the investigated $f_{ELM}$ range from 90 Hz-120 Hz. W is mainly eroded during the ELMs by energetic He ions with some moderate contribution (about 20%) of the Be ions.

In D plasmas, the in/out divertor asymmetry of the W erosion reduces significantly with the ELM frequency with a nearly symmetrical W erosion source in the inner and outer divertor areas at $f_{ELM}$ beyond 70 Hz. On the opposite, a strong in/out asymmetry is observed in He plasmas even at high ELM frequencies beyond 100 Hz. At $f_{ELM} \approx$ 100 Hz the outer divertor cross W source is larger by a factor of about 2.

In contrast to the intra-ELM phase, during the inter-ELM phase and Ohmic/L-mode, both species, Be and He, contribute to the W erosion in a ratio which depends on the divertor $T_e$: for the $E_{in} > 180$ eV the main sputter channel is due to $He^{2+}$ ions and for the $E_{in} < 180$ eV it is due to $Be^{2+}$. For twice ionised Be and He the $E_{in}$=180 eV corresponds to a $T_e$ of $\approx$ 22.5 eV. The contribution of the $He^+$ to W sputtering is negligible.

It is shown that calculated by SDTrimSP code sputtering yield curve for W can be well described by erosion due to $He^{2+}$ and 3.5% of $Be^{2+}$ ionic species. For the temperature range $T_e$ < 15 eV $Be^{2+}$ ions are solely responsible for the W erosion. Also a good agreement is found between the experimental intra-ELM yields and the theoretical yield curves.

The W sputtering and sources in the inter- and intra-ELM phases in the He plasmas are significantly larger than in D plasmas. The sputtering yield for He L-mode and inter-ELM plasmas is higher by a factor of 15-25 than in D plasmas. The ELM-induced W source in the outer divertor is more than a factor of 3 higher in the He plasmas in comparison with D plasmas.

It was shown that in He plasmas the Be erosion on the first wall is enhanced by the sputtering due to He ions resulting in the higher influx of Be. The beryllium concentration, measured by optical spectroscopy, is about 3.5% in the investigated plasma discharges and is larger than the

typical values of 0.5% in D plasmas. This in turn leads to an increase in the W erosion by means of Be ions in He discharges.

As already mentioned in the introduction, in order to develop plasma scenarios for the future deuterium-tritium (DT) operation as well as to commission the plasma diagnostics and the operationally relevant ITER systems, ITER consider a low activation phase with operation of H-modes in protium or helium plasmas [9]. The decision on which plasmas, He or protium (H), will be driven during this phase is not yet taken because of the shortage of results in He plasmas in the present tokamaks. It should be noted that during this learning, non-activated phase unmitigated ELMs are expected. As shown in this study W sputtering and sources are significantly larger in He than in D and they could seriously reduce the lifetime of the first wall components. We provide the ITER team with urgently needed information about the W erosion during the inter- as well as intra-ELM periods to take a decision on which plasma, He or H, will be preferred for the mentioned start-up phase.

DEMO is considered as the first fusion reactor power plant where a large amount of fusion alphas will be released in fusion reactions during the high performance deuterium-tritium (D-T) experiments. Tungsten is the prime candidate material for the first wall in DEMO, in the main chamber as well as in the divertor. To mitigate the risk of first wall damage, the reactor will likely be operated more in an ELM-free regime than in other regimes [40]. A helium concentration in the divertor of about 2-3% is expected in high-performance D-T plasmas. At such He concentrations, W erosion due the He particles will not be the main sputtering channel: significant W sputtering of the main wall will be caused by fast charge exchange (CX) neutrals; the erosion in the W divertor will be dominated by seeded impurity ions and self-sputtering [41].

## Acknowledgements

This work has been carried out within the framework of the EUROfusion Consortium and has received funding from the Euratom research and training programme 2014-2018 and 2019-2020 under grant agreement No 633053. The views and opinions expressed herein do not necessarily reflect those of the European Commission.

## References

[1] Pitts R A et al 2017 Nucl. Mater. Energy **12** 60
[2] Janeschitz G ITER JCT and HTs 2001 J. Nucl. Mater. **290-293** 1
[3] Jenkins H D B and Roobottom H K 2004 CRC Handbook of Chemistry and Physics 85th edn (Boca Raton, FL: CRC Press)
[4] Hirai T et al 2003 Phys. Scr. **T103** 59

[5] Ogorodnikova O et al 2003 J. Nucl. Mater. **313–316** 469
[6] Brezinsek S et al 2019 Nucl. Fusion **59** 096035
[7] Pütterich T. et al 2013 Plasma Phys. Control. Fusion **55** 124036
[8] Dux R et al 2009 J. Nucl. Mater. **390–391** 858
[9] Aymar R et al 2002 Plasma Phys. Control. Fusion **44** 519
[10] Brezinsek S et al 2015 J. Nucl. Mater. **463** 11
[11] Neu R et al 2013 J. Nucl. Mater. **438** S34
[12] Hakola A et al 2017 Nucl. Fusion **57** 066015
[13] Solano E R et al 2021 submitted to the Nucl. Fusion
[14] G. J. van Rooij et al., J. Nucl. Mater. 438 (2013) S42
[15] M. Laengner et al., J. Nucl. Mater. 438 (2013) S865
[16] S. Brezinsek et al., Phys. Scr. T170 (2017) 014052
[17] Den Harder N et al. 2016 Nucl. Fusion **56** 026014
[18] Abrams T et al 2019 Phys. Plasmas **26** 062504; doi: 10.1063/1.5089895
[19] Huber A et al 2020 Nucl. Mater. Energy **25** 00859; https://doi.org/10.1016/j.nme.2020.100859
[20] Solano E R et al 2017 Nuclear Fusion **57** 022021
[21] Kruezi U et al 2020 JINST 15 C01032
[22] Vartanian S, Delabie E, Klepper C C et al 2021 Fusion Eng. Des. **170** 112511
[23] Summers H P 2006 The ADAS User Manual, version 2.6 (www.adas.ac.uk/manual.php)
[24] Gervids V I et al 1987 Reviews of Plasma Physics **12**, ed. by M.A. Leontovich, B.B. Kadomtsev (Consultants Bureau, New York)
[25] Kallenbach A et al 2016 *Plasma Phys. Control. Fusion* **58** 045013
[26] Huber A and Chankin A V 2021 Nucl. Fusion 61 036049
[27] Mavrin A A 2017 Journal of Fusion Energy 36 161
[28] Mutzke A et al 2019 SDTrimSP Version 6.00 (IPP 2019-2) (Garching: Max-Planck-Institut für Plasmaphysik) (https://doi.org/10.17617/2.3026474)
[29] Eckstein W 2007 Sputtering Yields. In: Sputtering by Particle Bombardment. Topics in Applied Physics, vol 110. Springer, Berlin, Heidelberg. https://doi.org/10.1007/978-3-540-44502-9_3
[30] Morgan P D et al 1985 Rev. Sci. Instrum. **56** 862–4
[31] Meigs A et al 2010 Rev. Sci. Instrum. **81** 10E532
[32] Riemann K U 1995 IEEE Trans. Plasma Sci. 23 709 .
[33]Tokar M Z 1994 Contrib. Plasma Phys. 34 139
[34]Lee D, Hershkowitz N and Severn G 2007 Appl. Phys. Lett. 91 041505
[35] Stangeby P C 2000 The Plasma Boundary of Magnetic Fusion Devices (Bristol: Institute of Physics Publishing)
[36] Moulton D et al. 2013 Plasma Phys. and Control. Fus. **55** 085003
[37] Guillemaut Ch et al. 2018 Nucl. Fusion **58** 066006; https://doi.org/10.1088/1741-4326/aab7b1
[38] Borodkina I et al. 2020 *Phys. Scr.* **2020** 014027
[39] Tskhakaya D private communications
[40] Siccinio M et al., 2020 Fusion Eng. and Des. **156**, 111603
[41] A. Eksaeva et al, to be published in Physica Scripta